Accepted Manuscript

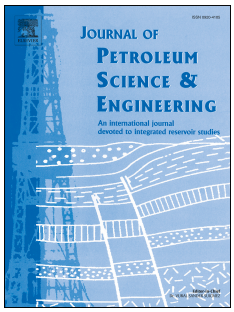

Proppant transport in a scaled vertical planar fracture: Vorticity and dune placement

Matías E. Fernández, Martín Sánchez, Luis A. Pugnaloni

PII: S0920-4105(18)30860-X

DOI: 10.1016/j.petrol.2018.10.007

Reference: PETROL 5370

To appear in: *Journal of Petroleum Science and Engineering*

Received Date: 11 July 2018

Revised Date: 25 September 2018

Accepted Date: 4 October 2018

Please cite this article as: Fernández, Matí.E., Sánchez, Martí., Pugnaloni, L.A., Proppant transport in a scaled vertical planar fracture: Vorticity and dune placement, *Journal of Petroleum Science and Engineering* (2018), doi: https://doi.org/10.1016/j.petrol.2018.10.007.

Proppant Transport in a Scaled Vertical Planar Fracture: Vorticity and Dune Placement

Matías E. Fernández[a,b], Martín Sánchez[b], Luis A. Pugnaloni[a]

[a] *Departamento de Ingeniería Mecánica, Facultad Regional La Plata, Universidad Tecnológica Nacional, CONICET, Avenida 60 Esq. 124, 1900 La Plata, Argentina.*
[b] *YPF Tecnología S.A. (Y-TEC), Av. del Petroleo Argentino s/n, 1923 Berisso, Argentina.*

Abstract

We report experimental results on the transport of proppant in a scaled planar cell. As a complement to many previous studies, we consider, apart from a proper scaling of the experimental cell and flow rate, a scaling of the perforations through which the fracturing slurry is injected. We also consider a fracture height relatively larger than usual, compatible with thick formations such as Vaca Muerta, Neuquén basin (Argentina). Under these conditions, we find that the flow pattern in the fracture presents large vortexes. The effect on the proppant transport is significant, yielding a much deeper placement of the dune than previously observed in similar experiments. We discuss the implications for the design of hydraulic fracturing operations.

Keywords: Proppant transport, Hydraulic stimulation, Multiphase flow

1. Introduction

Hydraulic fracturing is part of standard completion practices in shale

Email address: luis.pugnaloni@frlp.utn.edu.ar. Tel: +54 221 4124392 (Luis A. Pugnaloni)

formations to stimulate the production of hydrocarbons [1, 2]. One important aspect of this process is the packing of a propping agent that can keep the fracture open and conductive after completion, during the production life of the well. The granular materials used as proppants are expected to fill the fracture over a large extension, including the near wellbore area, and remain stable in place leaving a highly porous media through which the formation fluids can flow through into the wellbore [3]. These goals are often unmet due to a number of effects that impact the initial placement of the proppant (e.g., screening), its long-term stability (e.g., flowback) and/or its conductivity (e.g., spalling, embedding) [4].

Although there exist an extensive development of models for particle transport in fluids (for a review see [5]), the complexity of fluid flow in a fracture requires specific experimental and modeling studies [6]. A number of studies have considered experimental slot cells to model the transport of proppant in a planar fracture. In a pioneering work, Kern et al. [7] performed some of the first slot flow experiments. The cell consisted of a steel and acrylic slot (0.56 m $\times$ 0.19 m $\times$ 6.35 mm). The fluid (water and 20-40 mesh sand) was pumped to reach between 0.6 and 1.5 m/s. These velocities are actually above most estimations for a field operation, which are typically between 0.3 and 0.5 m/s [3, 8]. There are no explicit comments in their work regarding the way perforations were modeled; however, one may speculate that injection was made using a slot on the casing of the same height and aperture of the cell (i.e., 0.19m $\times$ 6.35mm) instead of perforations. The main conclusion of this study is that at high fluid velocities, proppant does not settle in the cell and is completely washed out. At lower velocities, a

settled dune develops soon after injection of the sand. The growth of the dune reduces the cross-section available to the flow, which induces an increase of the fluid velocity (at constant pumping rate). As a consequence, erosion is enhanced. Eventually, the balance between dune growth and erosion enhancement leads to an equilibrium height for the dune. The proppant injected at a later stage is dragged above the dune along a "traction carpet" and deposited farther downstream, leading to the horizontal growth of the dune. Based on these results, Kern et al. [7] suggested that the proppant that one desires to place closer to the wellbore (usually the larger mesh) should be injected first rather than last in the operation. A number of authors have reported similar results to those presented by Kern et al. [8–11]. However, there has been some skepticism regarding the extrapolation of these results to field operations where the traction carpet may never develop [12]. Most operations are still based on the "first in – deeper travels" assumption.

An important contribution to the knowledge of proppant transport has come in recent years by the experiments from the consortium lead by STIMLAB.[1] Their experiments on a vertical slot (2.44 m $\times$ 0.305 m $\times$ 8.0 mm) have confirmed some of the initial results by Kern et al. Most experiments reported in this setup consider, however, fluid velocities much lower than those studied by Kern et al. The maximum mean velocities in the fracture is about 0.1 m/s, which is one third to one forth of the expected mean velocities in a field operation [9–11]. In an earlier experiment [13], a much larger slot was used ((4.88 m $\times$ 1.22 m $\times$ 8.0 mm)). In this case, however,

[1] http://www.corelab.com/stimlab.

pumping rates were smaller and the mean fluid velocity was about 0.02 m/s. One important conclusion of this work was that vertical proppant velocities caused by convective motion, when fluids of different densities are pumped in consecutive stages, can be hundreds of times faster than single particle settling velocities. This was also pointed out a few years earlier by Cleary and Fonseca [14].

In a PhD dissertation, Liu [15] presented an apparatus designed to match the field Reynolds numbers. The system required a large positive displacement pump and instead of pumping uniformly across the fracture length, Liu used ten perforations that could be opened and closed to simulate different injection points that would mimic the perforation clusters created during the plug-and-perf operation. Although the precise dimensions of the perforations are not reported, the jet velocity achieved suggests that these were somewhat large compared to the relative height of the fracture. Nevertheless, the experiments by Liu are possibly closer to a realistic scaling than most others. Apart from the effect of traction carpet, Liu emphasized that when pumping through only one or two perforations, the flow developed large eddies that erode the sand from the initial part of the cell, leaving the propped region disconnected from the wellbore.

More recently, Sahai et al. [8] have presented results consistent with those of Kern et al. and STIM-LAB. Moreover, these authors have considered complex geometries with branching fractures. In the main vertical slot (1.22 m $\times$ 0.61 m $\times$ 5.5 mm), the fluid and particles are injected through various injection inlets, reaching a maximum mean fluid velocity in the cell of 0.33 m/s. This is one of the few studies, apart from the work of Liu,

where mean fluid velocity is similar to the one expected in field operations, and this has been achieved thanks to a previous design where model scaling was central. The dimensions chosen for the inlet perforations has not been specified and there is not a specific discussion on their scaling. One may have expected that these experiments reported large eddies, however the authors do not seem to consider this phenomenon somehow important.

Other studies have considered vertical cells of different sizes and used different fluid velocities. In general, mean fluid velocities are smaller than recommended by proper scaling and the scaling of the perforations is disregarded. Malhotra et al. [16] considered a small cell with mean fluid velocity around 0.037 m/s. Kadhim et al. [17] developed a cell where they did not have proper control on fluid velocity. Ferández et al. [18] did not exceed 0.1 m/s in fluid velocity in a small cell (although they did use small injection perforations). Ray et al. [19] focused on the bridging phenomenon using a small scale cell, but they worked at low fluid velocities of about 0.01 m/s.

One important aspect for the flow pattern is the actual height of the fracture. Most previous studies have considered long but not too tall slots. This may be reasonable when considering some thin formations. However, for thick formations, such as the Vaca Muerta shale, Neuquén basin (Argentina), fractures can be significantly tall [20]. In tall fractures, effects like traction carpet can be difficult to achieve and probably only a portion of the fracture height can be effectively propped.

In this work, we pay special attention to the scaling of the mean fluid velocity, both in the cell and in the perforation clusters. We also consider a rather tall fracture in comparison with most studies. The resulting device

requires pumping the fluids at a high pressure into the casing to achieve the required flow rates through rather small perforations in comparison with previous works. These experimental conditions are particularly unique since scaling of perforation clusters has not been considered before. We study the transport and placement of sand proppant at different fluid velocities and for different duration of the fracturing treatment. We find that the dynamics in the cell presents large vortexes, with local velocities significantly exceeding the mean fluid velocity. These vortexes dominate the proppant transport along a large portion of the cell length. We analyze the size, shape and position of the settled dunes. At low pumping rates, our results are consistent with those from Sahai et al. [8] and Liu [15]. However, for pumping rates compatible with usual field operations, most proppant is washed out and transported deep into the fracture, beyond the limits of the region simulated in the experiment. Since these types of proppant transport laboratory devices are significantly idealized, we added to the fracture some degree of roughness and tortuosity. The preliminary finding is that the vorticity observed in smooth slots is remarkably reduced and settling is much more significant.

2. Model scaling

During the design of laboratory experiments that aim at mimicking a real fracture, the scaling is an essential step to warrant that the flow patterns observed comply with kinematic and dynamical similitude [21]. The scaling of these type of experiments has been discussed previously by others [1, 8]. However, little stress has been put on the implications of the scaling decisions made and how the results should be interpreted considering the scaling. In

this section we discuss this with some detail since this will become crucial when interpreting the results and in the comparison with results of similar experimental devices described in the literature.

There is a special complexity associated to the scaling of a hydraulic fracture with the goal of proppant transport studies. Since the proppant and the fluid generally used for the tests in the laboratory will be the same as the ones used in a field operation, the aperture of the model fracture cannot be scaled down. As a consequence, the height and length of the fracture is scaled while the width is conserved to keep the same ratio between the particle size and the fracture aperture. Despite this limitation, as long as the length and height remains much larger than the aperture, the correct dynamic scaling can be achieved since the laboratory cell will still correspond to a parallel plates configuration (akin a Hele–Shaw cell). In addition, if different fluids are used in consecutive stages, scaling must consider the effect of convection due to fluid density gradients since convection is much faster than particle settling [14]. We will not consider this effect since only one type of fluid will be used in the tests.

To comply with dynamical similarity, we will require that the Reynolds number (Re) for the fluid in the parallel plates configuration, for the particles and for the perforations used for injection must be the same as in the field.

2.1. Reference fracture.

As a reference, we set a series of dimensions for a field operation that we aim at modeling in the laboratory. We consider a planar fracture in a very low permeability formation (e.g., a shale) with a constant thickness of 6.0 mm. The half-wing length is set to 80.0 m and the height to 40.0 m. The

height selected is a few times larger than used by other author. This is due to the interest in modeling fractures usually attained in the Vaca Muerta formation (Neuquén, Argentina). We assume the fracturing fluid is pumped at a constant flow rate of 0.16 m^3/s (i.e., $\approx$ 60 bpm) which is divided in half to feed each half-wing. This results in a mean fluid velocity of 0.33 m/s in the fracture. In addition, we will scale the laboratory device to inject the fluids through two small regions compared to the fracture height to model the perforation clusters. We assume that each cluster has 38 perforations of diameter 0.38 in. Then, the total cross-section through which the fluid is injected in each cluster, assuming all the perforations are active, corresponds to 2784 mm^2. Table 1 summarizes the field dimensions.

2.2. Re for the parallel plates.

All the experiments carried out in this study use fresh water as the transport fluid.

The Reynolds number for a parallel plates configuration is defined as $Re_{\text{frac}} = \rho v 2e/\mu$ for a Newtonian fluid with dynamic viscosity μ. Here, e is the plates separation, ρ is the fluid density and v is the velocity of the fluid parallel to the plates. Hence, if one utilizes the same fluid as in the field and the fracture aperture e is the same as in a realistic fracture, the same Re_{frac} will be obtained by simply setting the mean fluid velocity parallel to the plates equal to the field mean velocity. For the reference field dimensions described above, the mean velocity in the fracture is about 0.33 m/s. Therefore, the flow rate Q' needed to set this mean velocity in the experimental cell will be

$$Q' = e \times h' \times 0.33 \text{ m/s}; \quad (1)$$

being h' the height of the scaled cell.

Table 1 shows that the scaling of the pumping rate warrants that Re_{frac} be the same in the field and in the scaled cell. We have to bear in mind that a field operation will inject fluid into two half-wings, while our scaled cell in the lab will only represent one half-wing.

2.3. Re for the particles.

The particle Reynolds number in a Newtonian fluid is defined as $Re_{\text{part}} = \rho v d/\mu$, where d is the particle diameter and v its velocity with respect to the fluid. Again, since the proppant particles will be the same as those used in field operations, this Re in the lab is simply obtained by using the same conveying fluid and the same velocities v, as discussed in section 2.2.

2.4. Re for the perforations.

One more Reynolds number, generally disregarded in the literature, appears to be relevant in this scaling. The injection into the fracture occurs through a narrow section of the fracture height: the perforation cluster. As a result, the fluid dynamics in the fracture is very complex close to the perforations and cannot be thought of as a smooth velocity profile across the height of the fracture. This is an important feature to be considered during the analysis of the results in the following sections. We will show that the complex dynamics of the fluids in the fracture extends far beyond the distances expected in most simple models and also the distance observed in laboratory experiments available in the literature.

The Reynolds number for any perforation, considered as a pipe, is defined as $Re_{\text{perf}} = \rho v d_{\text{perf}}/\mu$, for a Newtonian fluid, with d_{perf} the diameter of the perforation and v the velocity of the fluid.

In practice, a few clusters of perforations are stimulated simultaneously at each stimulation stage. In vertical boreholes, two neighbor perforation clusters may connect to the same vertical fracture. We have modeled each perforation cluster (two in our case) as a single inlet perforation each. These circular inlets have a cross section which conserves the same proportion (about 170) with the cell cross section as the proportion of perforated area in the casing versus the field fracture cross section (two half-wing). In doing this, we create injection regions that are of the same size as the real perforation clusters when compared with the entire fracture. However, in the field, the fluid is not pumped through a single orifice but through a number of small orifices at each cluster. This makes the laboratory Reynolds number at the perforations somewhat smaller than in each real perforation. Nonetheless, the Reynolds numbers are still in the same highly turbulent regime (see Table 1). The fluis velocities we achieve in the perforations (> 28 m/s) are much higher than the values reported by Liu [15].

2.5. Other nondimensional quantities

A number of relevant nondimensional parameters (other than the Reynolds numbers) can be shown to be conserved in the experiments if the proppant particles, carrying fluid, cell width and mean fluid velocity are the same as in the field [1, 9]. In Table 1, we include the values for the Buoyancy number ($Bu = \frac{\rho g e}{\mu \dot{\gamma}}$), the Shields number ($\theta = \frac{\tau}{(\rho_{\text{p}} - \rho) g d}$), the particle-to-fluid density ratio (ρ_{p}/ρ), the Stokes-to-Froude ratio ($St/Fr^2 = \frac{mg}{6\pi d \mu}$) and the fracture

height-to-length ratio (h/L). Here m is the proppant particle mass, ρ_{p} is the material density of the proppant, g is the acceleration of gravity, $\dot{\gamma} = v/e$ is the shear rate and $\tau = \mu v/e$ is the shear stress on a deposited granular bed (estimated following Ref. [9]).

2.6. Length and time scales.

Our laboratory cell is scaled 1:50 in the horizontal (x) and vertical (y) directions with respect to the reference fracture. As we mentioned, the aperture e of the slot is the same as the field fracture: 6 mm. Then, the cell cross section ($e \times h$) is reduced 50 times. The pumping rate will be reduced 100 times to conserve the mean fluid velocity in the cell. Again, note that only one half-wing of the fracture is simulated. As we discussed above, this warrants that the Reynolds numbers are equivalent to the ones in the field (see Eq. (1)).

In the direction perpendicular to the cell plane (the z-direction), the length scales are conserved. However, in the xy–plane a single proppant particle covers a relative area $50 \times 50 = 2500$ times larger than the same particle in the reference fracture. The typical amount of fluid and proppant needed for the model is therefore 2500 times smaller than in the field operation.

The field fracture and the laboratory model are kinetically similar; i.e., the ratio between the fluid velocity in two corresponding points (field and model) is always the same. In our case, this ratio is 1 (one). Hence, the velocity in the vicinity of the model perforations match the one observed in the field, and the same is true in any other place of the cell. However, the horizontal and vertical length scales have been reduced 50 times. As a consequence, the time scales ($T = L/V$) are also reduced 50 times with

respect to the field operation. In practice, this means that a full operation that takes 100 min in the field will be accomplished in 2 min in the laboratory cell. Hence, to appreciate the kinematic effects in the video of a laboratory experiment in terms of real fracture scales, the record has to be played at 1/50 speed.

3. Experimental

3.1. Experimental apparatus.

Figure 1 shows a drawing to scale of the experimental device. The cell consist in two vertical parallel acrylic plates (25.0 mm thick) separated by a stainless steel frame (the inner perimeter is 1600 mm long and 800 mm high). The acrylic plates are slimmer on the edges to allow them to fit into the frame and leave a gap of 6 mm between them inside the frame. An elastomeric seal is used between the frame and the plates. The frame has two inlet perforations (6 mm in diameter) at 350 mm and 450 mm from the base. The outlet side has 49 perforations (6 mm in diameter) distributed along its height. Every 7 outlet orifices, a collector redirects the exiting fluid to a sink tank. The inlet side of the stainless steel frame is welded to a 2 in stainless steel pipe that serves as casing. The two acrylic plates are sustained in position by two metallic matrices of 60 mm in thickness. These matrices avoid the cell to deform under pressure during the experiments. The parallel plates with the matrices were tested to deform a maximum of 0.2 mm during the tests. Hence, the aperture of the cell is conserved within 7 %. We have checked that the gap between the parallel plates is correct by measuring the cell volume filling it with water.

The slurry is injected into the cell through the casing and inlet perforations by a peristaltic pump (Verderflex Dura-45). Due to the relatively high flow rate required to be pumped through the small perforations, the casing pressure rises up to 12 Kg/cm^2. The selected pump is a positive displacement pump that allows a defined flow rate to be delivered up to differential pressures of 16 Kg/cm^2.

The pump is fed from a blender where the fluid and proppant are mixed using a rotating blade with controlled velocity. A system of pneumatic valves is used to swap between slurry and fresh water supply to the pump. Since the peristaltic pump delivers a pulsed flow, a flow damper is used after the pump to deliver a continuous flow rate to the cell. A flow meter and two pressure gages are used to monitor flow rate and cell pressure during the experiments. At the drainage, a fabric filter is used to collect the exiting proppant and so measure the amount placed beyond the length of the cell. We have controlled that the flow rate set to the pump is indeed achieved according to our flow meter in each run.

Video recordings of the cell during each experiment are taken using a digital camera at 120 frames per second with full HD resolution. After pumping is stopped and proppant has fully settled, an image is taken at 4032×3024 pixel resolution. To reduce the exposure time at high speed recording, two white LED lights (250 W, 22500 lumen each) and light diffusers are used.

In a few exploratory experiments, we have used a "rough" and "tortuous" slot. In this case, two acrylic plates where mechanized using a CNC router; one being complementary (negative) to the other. The separation between the plates is kept at 6 mm in the z-direction. Each plate has the shape of

a two-dimensional harmonic function ($\sin x \sin y$) with wavelength 200.0 mm and pick-to-pick amplitude 9.0 mm. On top of this long wavelength shape, 3.0 mm-deep grooves are created along the vertical y-direction every 5.0 mm to mimic some roughness. An image of one of the rough plates can be seen in Fig. 6. Thanks to the close refraction index of water and the acrylic used, transparency is only marginally affected by the rough surfaces.

3.2. Experimental protocols.

An experimental run consist of a series of steps. Firstly, the cell and the pipes must be purged. The purges valves are opened and water is pumped through the cell at a low rate until the cell is full of water. A few valves of the drain need to be closed so that the pressure inside the cell rises and the air can be removed through the purge valves. This procedure is repeated at higher flow rate until the desired pumping rate for the experiment is achieved and there is not visible air in the cell. Then, the purge valves are closed, the drain valves opened and the pressure gage and flow meter recording started.

Secondly, the fracturing fluid is prepared. Water is placed in the blender with its outlet valve closed. The blender motor is started and set to the lowest possible frequency that warrants that most proppant will be kept in suspension in the blender. Proppant is placed through the loading mouth of the blender in the desired proportion. In some experiments, a continuous feeding of water and proppant is used since the blender capacity is limited.

Thirdly, we configure the flow rate in the peristaltic pump frequency inverter to the desired value. The flow damper, with its isolation valve closed, is pressurized at the calibrated pressure required for the flow rate chosen.

Finally, the pump is turned on, pumping only water for about 10 s. Then,

the isolation valve of the flow damper is opened and the flow is left to stabilize (approximately 5 s). Only then, the pneumatic valves from water tank and blender are inverted and the fracturing fluid is allowed to be pumped into the cell. After the entire volume of the mixture is evacuated from the blender, the pneumatic valves are inverted again to pump further water through the pipes and ensure that no fracturing mixture is left in the pipes. The peristaltic pump is stopped right after observing that proppant injection in the cell has ceased, avoiding any over-flush.

Recording of the cell is started just before initiating the proppant injection and stopped after full settling of the particles. Depending on the flow rate and amount of proppant injected, the total injection time varies between 12 s and 100 s. Scaling to field operations, this corresponds to 10–83 min.

4. Results

All the experiments were carried out using as proppant a natural sand (mesh 30/70, apparent bulk density 1520 kg/m^3). The proppant concentration used in the mixture was 0.5 kg/l (about 2.0 lb/gal). We have varied the flow rate and total amount of fluid injected. The relevant quantities for each experiment are listed in Table 2. The lower flow rate scales to the reference field operation to 40 bpm, the higher flow rate to 62 bpm. We recall here that flow rate has been scaled down 50 times and also only half-wing of the fracture is simulated.

4.1. Flow pattern.

Figure 2 shows a series of snapshots during one experimental run. For this particular flow rate (61.0 l/min), some of the features already described

in the literature are apparent. For example, some proppant settles during pumping and a dune forms. Part of the proppant injected later seems to overcome the initial dune and deposit deeper into the fracture as described by others [7–9, 15]. However, the flow pattern is very complex in agreement with the early discussion by Liu [15]. Due to the scaled perforation through which the fluid is injected, large vortexes are created in the cell since strong narrow streams enter into a large section. These vortexes are active along the entire length of the cell. In contrast, in Liu's work, the complex flow only covered the initial part of the cell. We believe our cell is more affected by turbulence due to the fact that the entering jet velocities are seven times higher and the cell is twice as high as Liu's cell. A clear recirculation is observed along the top edge of the cell and at the bottom right corner. We do not see a clear homogeneous flow profile. Such homogeneous profile may develop further downstream, but our cell is not long enough to capture this.

Given that our cell and perforations were designed to attain kinetic similitude, one should expect a similar flow pattern to be present in a field operation. This would mean that, typically, for a 40 m high fracture, the flow pattern is rather complex at least during the initial 80 m of the fracture length. Due to the vortexes, the fluid velocity is well above the mean flow velocity in several regions, which leads to stronger sand erosion than it may be expected. To better show this effect, a movie is provided as supplemental material.[2] This movie has been slowed down to scale (1:50) so that the

[2]Video of the experimental run for a flow rate of 61.0 l/min where 25 kg of proppant has been injected. The video is played at 1/50 speed to observe the dynamics scaled to a real fracture (see section 2). The video can be accessed at http://(to be inserted by

velocities observed are in accordance to a field fracture scale.

It is important to bear in mind that a field fracture will present some degree of roughness and tortuosity. This may change significantly the flow pattern. However, if one compares results of previous studies made with smooth cells at lower pumping rates or without a scaling of the perforations, the flow pattern is markedly different. In section 4.4, we will show some preliminary indications of the effect of roughness and tortuosity.

An additional important point in the flow pattern observed is the positioning of the inlet perforations [15]. We have placed the perforations at a central position with respect to the fracture. A different placement may lead to a different configuration of the vortexes that may change the proppant transport to a large extent. The entire process seems to be very much determined by these vortex configuration. Notice however that this pattern of the flow will develop as proppant is deposited and the resulting dune changes the effective geometry of the cell. An simulation study of the effect of perforation placement for the initial stages of the operation can be seen in Ref. [22].

4.2. Deposited dune.

Figure 3 shows the final deposited dune after 25 kg of proppant has been injected at different flow rates. This is equivalent to a field operation of about 83 min for the lowest (or 50 min for the highest) pumping rate studied. The lower-right panel of Fig. 3 shows the extracted dune profiles for comparison. As we can see, the lower the pumping rate, the larger is the final deposited dune in the cell. For the high flow rates, most proppant is displaced beyond

editor).

the limits of the cell through the outlet perforations. As it is expected, the deposited dune is placed closer to the inlet perforations as the flow rate used is reduced. However, the large vortexes in the cell tend to wash the first half of the cell length, leaving only a small heap next to the casing thanks to a low velocity region in the lower right side of the cell.

It is important to mention that the small heap (approximately 20 cm high) observed at high pumping rates (compatible with 60 bpm) corresponds to a height of 10 m in the field. At the highest pumping rate, Liu observed that the developed dune equilibrates at a height of 8 m. Although the final results seem similar, in Liu's work the gap between the dune and the ceiling of the cell is very narrow (3 m at field scale), having then propped most of the fracture height. In effect, for our tall fracture, a high pumping rate prevents us to take full advantage of propping the entire height of the formation.

In Fig. 4, we present images of the final dune after different amounts of proppant have been injected using the lower flow rate (61.0 l/min). The injection of a small quantity of proppant does not generate a heap but a somewhat flat sand bed. Despite the erosion expected due to the vortexes close to the casing, the proppant does not really settle during the short experiment. After turning off the injection, the suspended sand settles rather homogeneously in the cell. If the amount injected is larger, the experiment last longer and the sand settles partially during the injection phase. A heap forms and grows at about three quarters of the length of the cell. In terms of the field reference fracture, this would position the tip of the dune at about 60 m from the wellbore. The height of the dune increases with the amount of proppant. Interestingly, a vortex close to the injection points erodes the

sand bed and depletes the near wellbore area. In fact, injecting a moderate amount of proppant seems to be beneficial to avoid the depleted region close to the perforations.

4.3. Area of deposited dune.

Despite the different dune shapes and positions observed in the experiments, one key parameter to assess the quality of an operation is the total area of the fracture effectively covered by the deposited dune. In Fig. 5, we show the fraction of the total cell area covered by the proppant as a function of flow rate (a) and as a function of total amount of proppant injected (b). As it can be expected, the higher the flow rate, the lower the area of the dune. However, the proppant that left the cell through the exit perforations are effectively covering deeper parts of the fracture in a real operation. The values reported here are in fact an indication of the area covered in the first 80 m of the fracture length.

When we focus on the area of the dune as a function of the total amount of proppant injected, we also see an important increase (Fig. 5b). However, this increase is mild and saturates quickly for the higher injection rates. This indicates that for 60 bpm pumping, the amount of sand deposited in the initial 80 m of the fracture is small and independent of the duration of the operation.

4.4. Effect of roughness and tortuosity

Our results with a smooth planar cell suggest that results of previous studies may not be representative of real operations since the high fluid velocities required were not achieved or the perforations were not scaled. However, the

high vorticity obtained in these experiments may be also unrealistic since other simplifications are dramatic in the laboratory cell. One such simplification is the smooth character of the cell and the direct entrance of fluid to the slot though the perforations. Actual fractures are not perfectly planar nor smooth. We have used the rough slot described in section 3.1 to asses in a qualitative fashion the effect that this may have on the complexity of the flow profile.

Figure 6 shows the progression of the flow profile in a test with the same pumping rate and proppant concentration as in Fig. 2 but using the rough slot. As we can see, the complex eddies observed in Fig. 2 are not apparent. The flow looks much more homogeneous despite some recirculation is clear at the top-right corner of the cell. The transport is much less efficient, in the sense that a larger proportion of the proppant settles in the cell before leaving though the outlet perforations.

The settling observed in the rough slot looks qualitatively similar to the one shown by previous studies where smooth slots are used, although with a much lower fluid velocity than recommended by proper scaling. Previous laboratory results may sound reasonable, but this may be caused by an error compensation. The smooth slot allows for an unrealistic deep placement of the proppant, but this is compensated by the use of a too low flow velocity.

5. Conclusions

Propping the near wellbore area is critical to avoid "pinch-out". Pinch-out is the phenomenon that leads to the closure of a section of the fracture close to the wellbore that isolates a well-propped area from the casing. To

warrant a conductive fracture all the way back to the casing, a proper understanding of the dynamics of the fracturing slurry in the initial sections of the fracture, close to the perforations, is very valuable. In this work, we have put special attention at scaling not only the experimental slot cell and flow rate but also the perforations. In this way, we can assess the expected dynamics along the initial 80 m of a reference fracture compatible with those observed in thick shale formations.

The dynamics observed in our experiments indicate that at the usual operation pumping rates (60 bpm), the fluid will develop large vortexes that extend over a long distance and height, creating a very complex pattern. A more homogeneous flow profile may be observed far deeper into the fracture (beyond 80 m). This strongly turbulent dynamics washes out the proppant (for the tested 30/70 natural sand), dragging most of the material deep into the fracture. Moderate pumping rates (equivalent to 40 bpm in the field) will however create a tall dune at about 60 m from the perforations. These results fill a gap in view of other experiments that explore different regimes, where fluid velocities are about one order of magnitude smaller [9–11], where perforations have not been scaled [7–9, 15].

Despite the previous conclusions drawn for smooth planar slots with proper scaling, realistic fracture models should include other details that may affect significantly these observations. In particular, we have considered, in an exploratory fashion, the effect of roughness and tortuosity. The observed vorticity and deep proppant placement seems to be strongly affected. This suggest that much more research is necessary before scaled fracture experiments can be used to make sound predictions on field operations.

Acknowlegments – We are indebted to J. P. Cagnola, J. P. Peralta and V. S. Sacchetto (Universidad Tecnológica Nacional, Facultad Regional La Plata) for their help in the technical design and construction of the experimental device. We acknowledge discussions with A. Guzzetti, W. Morris, S. Marco, and F. Castez (Y-TEC SA). The appreciate the suggestions and comments received from E. D'Huteau, M. Vitolo and S. M. Giovagnoli (YPF SA). This research has been possible thanks to the funding provided by Y-TEC SA.

[1] Barbati, A.C., Desroches, J., Robisson, A., McKinley, G.H., 2016. Complex fluids and hydraulic fracturing. Annu. Rev. Chem. Biomol. Eng. 7, 18.1-18.39.

[2] Detournay, E, 2016. Mechanics of hydraulic fractures. Annu. Rev. Fluid Mech. 48, 311-39.

[3] Osiptsov, A.A., 2017. Fluid mechanics of hydraulic fracturing: A review. J. Petroleum Sci. Eng. 156, 513-535.

[4] Economides, M.J., Martin, T., 2007. Modern fracturing: Enhancing natural gas production. ET Publishing, Houston, TX.

[5] Soepyan, F.B., Cremaschi, S., Sarica, C., Subramani, H.J., Kouba, G.E., 2014. Solids transport models comparison and fine-tuning for horizontal, low concentration flow in single-phase carrier fluid. AIChE 60, 76-122.

[6] McLennan, J.D., SaGreen, S.J., Bai, M., 2008. Proppant placement during tight gas shale stimulation: Literature review and speculation. In: ARMA 08-355, 42nd US Rock Mechanics Symposium and 2nd U.S.-Canada Rock Mechanics Symposium, San Francisco, June 29- July 2.

[7] Kern, L.R., Perkins, T.K., Wyant, R.E., 1959. The mechanics of sand movement in fracturing. J. Pet. Technol. 11, 55-57.

[8] Sahai, R., Miskimins, J.L., Olson, K.E., 2014. Laboratory results of proppant transport in complex fracture systems. In: SPE 168579, SPE Hydraulic Fracturing Technology Conference, The Woodlands, Texas, 4-6 February.

[9] Patankar, N.A., Joseph, D.D., Wang, J., et al., 2002. Power law correlations for sediment transport in pressure driven channel flows. Int. J. Multiphase Flow 28, 1269-1292.

[10] Wang, J., Joseph, D.D., Patankar, N.A., et al., 2003. Bi-power law correlations for sediment transport in pressure driven channel flows. Int. J. Multiphase Flow 29, 475-494.

[11] Woodworth, T.R., Miskimins, J.L., 2001. Extrapolation of laboratory proppant placement behavior to the field in slickwater fracturing applications. In: SPE 106089, SPE Hydraulic Fracturing Technology Conference, College Station, Texas, 29-31 January.

[12] Medlin, W. L., Sexton, J. H., Zumwalt, G. L., 1985. Sand transport experiments in thin fluids. In: SPE 14469, SPE 60th Annual Technical Conference and Exhibition, Las Vegas, Nevada, 22-25 September.

[13] Barree, R.D., Conway, M.W., 1994. Experimental and numerical modeling of convective proppant transport. IN: SPE 28564, SPE 69th Annual Technical Conference and Exhibition, New Orleans, Louisiana, 25-28 September.

[14] Cleary, M.P., Fonseca, A., 1992. Proppant convection and encapsulation in hydraulic fracturing: Practical implications of computer and laboratory simulations. In: SPE 24825, SPE 67th Annual Technical Conference and Exhibition, Washington, DC, 4-7 October.

[15] Liu, Y., 2006. Settling and hydrodynamic retardation of proppants in hydraulic fractures. PhD thesis, The University of Texas at Austin.

[16] Malhotra, S., Lehman, E.R., Sharma, M.M., 2014. Proppant placement using alternate-slug fracturing. SPE J. 19, 974-985.

[17] Kadhim, D.A., Imqam, A., Dunn-Norman, S., 2017. Ceramic proppant transport and placement in heterogeneous fracture systems. In: Unconventional Resources Technology Conference (URTEC), Austin, Texas, 24-26 July, pp. 3517-3534.

[18] Fernández, M.E., Baldini, M., Pugnaloni, L.A., Sánchez, M., Guzzetti, A.R., Carlevaro, C.M., 2015. Proppant transport and settling in a narrow vertical wedge-shaped fracture. In: ARMA 2015-135, 49th US Rock Mechanics/Geomechanics Symposium, San Francisco, California, 28 June-1 July.

[19] Ray, B., Lewis, C., Martysevich, V., Shetty, D.A., Walters, H.G., Bai, J., Ma, J., 2017. An investigation into proppant dynamics in hydraulic fracturing. In: SPE 184829-MS, SPE Hydraulic Fracturing Technology Conference, The Woodlands, Texas, 24-26 January.

[20] Ortiz, A.C., Hryb, D.E., Ramirez Martínez, J., Varela, R.A., 2016. Hydraulic fracture height estimation in an unconventional vertical well

in the Vaca Muerta Formation, Neuquén basin, Argentina. In: SPE 179145-MS, SPE Hydraulic Fracturing Technology Conference, The Woodlands, Texas, 9-11 February.

[21] Fox, R., 2004. Introduction to fluid mechanics, Wiley, New York.

[22] Baldini, M., Carlevaro, C.M., Pugnaloni, L.A., Sánchez, M., 2018. Numerical simulation of proppant transport in a planar fracture. A study of perforation placement and injection strategy. Int. J. Multiphase Flow (in press) https://doi.org/10.1016/j.ijmultiphaseflow.2018.08.005.

Figure 1: Drawing of the experimental device (to scale): (1) Peristaltic pump and flow damper, (2) fresh water tank, (3) blender, (4) flow meter, (5) cell, (6) pressure gages (and purge valves), (7) supporting table, (8) drainage.

Figure 2: Snapshots of an experimental run for a flow rate of 61.0 l/min where 25 kg of proppant has been injected through the right perforations. In the reference field fracture this corresponds to pumping at 40 bpm a 30/70 natural sand at 2.0 lb/gal concentration during 83 min. The final settled dune contains about 9.1 kg of proppant, the rest having been transported through the outlet perforations. The labels indicate the time elapsed since the initial injection of sand. The final snapshot was taken after turning off the pump and letting the proppant settle down. See also the full video provided as supplemental material.

Figure 3: Images of the final dune for different flow rates as indicated in the legends. These flow rates correspond in the reference fracture to: 38 bpm, 45 bpm, 52 bpm, 58 bpm and 63 bpm. (Bottom-right) Profile of the final dune in each image.

Figure 4: Images of the final dune for different total amount of proppant injected as indicated in the legends. (lower-right) Profile of the final dune in each image.

Figure 5: Percentage of the cell covered by the deposited proppant as a function of the flow rate (a) and as a function of the amount injected proppant (b).

Figure 6: (upper left) Photograph of the inside of one of the plates of the rough cell. Snapshots of an experimental run using the rough slot for a flow rate of 61.0 l/min where 25 kg of proppant has been injected through the right perforations. These are the same conditions as in Fig. 2. The final settled dune contains about 12.5 kg of proppant (compare with the 9.1 kg in Fig. 2), the rest having been transported through the outlet perforations. The labels indicate the time elapsed since the initial injection of sand. The final snapshot was taken after turning off the pump and letting the proppant settle down.

Table 1: List of dimensions for the field reference fracture and the laboratory cell.

Property	Field		Lab. cell (half-wing)	
Fracture height	40.00	m	0.80	m
Fracture half-wing length	80.00	m	1.60	m
Fracture width	6.00	mm	6.00	mm
Perforation clusters	2		2	
No perf. per cluster	38		1	
Perforation diameter	9.65	mm	6.00	mm
Effective cluster cross section	2779	mm^2	28.27	mm^2
Pumping rate	0.16	m^3/s	0.0016	m^3/s
Mean velocity in fracture	0.33	m/s	0.33	m/s
Mean velocity in perforation	28.79	m/s	28.29	m/s
Fluid density (ρ, water)	1000	kg m^{-3}	1000	kg m^{-3}
Fluid viscosity	0.001	kg m^{-1} s^{-1}	0.001	kg m^{-1} s^{-1}
Operation time	60	min	72	s
Re fracture (water)	3300		3300	
Re perforation (water)	2.8×10^8		1.6×10^5	
Bu (water)	10.69		10.69	
θ (water and 30/70 sand)	0.92		0.92	
ρ_p/ρ (water and 30/70 sand)	2.533		2.533	
St/Fr^2 (water and 30/70 sand)	0.0011		0.0011	
Fracture height/fracture length	0.5		0.5	
Fracture/cluster cross section	173		170	

Table 2: Conditions of the experiments. The two last columns indicate the total amount of proppant and water pumped in the fracturing mixture, respectively.

N	Flow rate [l/min]	Proppant [kg]	Water [l]
1	61.0	5.0	20
2	61.0	10.0	40
3	61.0	15.0	60
4	61.0	20.0	80
5	61.0	25.0	100
6	72.2	5.0	20
7	72.2	10.0	40
8	72.2	15.0	60
9	72.2	20.0	80
10	72.2	25.0	100
11	83.4	5.0	20
12	83.4	10.0	40
13	83.4	15.0	60
14	83.4	20.0	80
15	83.4	25.0	100
16	91.7	5.0	20
17	91.7	10.0	40
18	91.7	15.0	60
19	91.7	20.0	80
20	91.7	25.0	100
21	100.0	5.0	20
22	100.0	10.0	40
23	100.0	15.0	60
24	100.0	20.0	80
25	100.0	25.0	100